Making SABRE Enhanced Low-Field NMR Experiments Accessible to Modern Research Labs

A Technical Report submitted to the Department of Biomedical Engineering

Presented to the Faculty of the School of Engineering and Applied Science
University of Virginia • Charlottesville, Virginia

In Partial Fulfillment of the Requirements for the Degree
Bachelor of Science, School of Engineering

Clark Eriksson
Spring, 2021

Technical Project Team Members
Clark Eriksson

On my honor as a University Student, I have neither given nor received unauthorized aid on this assignment as defined by the Honor Guidelines for Thesis-Related Assignments

Making SABRE Enhanced Low-Field NMR Experiments Accessible to Modern Research Labs

Clark W. Eriksson[a,1]. Warren S. Warren[b]

[a] Department of Biomedical Engineering, University of Virginia, Charlottesville, VA, 27704
[b] Department of Physics, Chemistry, Biomedical Engineering, and Radiology, Duke University, Durham, NC, 27708
[1] Correspondence: cwe5gc@virginia.edu, 2019 Spring Creek Dr. Durham, NC 27704, (703)638-4555

Abstract

Magnetic Resonance Imaging (MRI) is an important and rapidly developing clinical imaging technique. However, it is fundamentally limited by low signal intensities which makes large magnetic fields necessary to produce clear images. Traditionally this low sensitivity has been addressed by using increasingly large magnetic fields to generate signal. However, because of high cost of care and acquisition and rapidly depleting cryogen resources for cooling these powerful magnets, lower field alternatives are being investigated. Low field imagers would be less costly for hospitals to purchase and maintain and would increase access to the powerful diagnostic information available with this imaging technique. Advances in post-acquisition processing and pre-acquisition sample preparation have expanded the possibilities of using low field MRI in a clinical setting. Here, I focus on improving the accessibility of a newly introduced hyperpolarization technique which creates large spin polarizations and therefore large MR signals without the need for high magnetic fields: Signal Amplification By Reversible Exchange (SABRE). SABRE hyperpolarization uses an iridium catalyst to connect highly polarized parahydrogen with a target nucleus to transfer polarization from the parahydrogen spin state to the target. This technique is complicated by many experimental variables which can be difficult to experimentally optimize. By creating a user interface for a newly introduced numerical simulation package which accurately predicts polarization dynamics in SABRE experiments and coupling that interface with a rigorously reproducible electromagnet coil array, I establish an experimental protocol which makes low-field SABRE experiments more easily accessible and less variable for use in any basic Nuclear Magnetic Resonance (NMR) laboratory. This apparatus and theoretical optimization of NMR pulse parameters opens up the opportunity to increase the scientific inquiry into this relatively young hyperpolarization technique with the aim of improving our understanding of this regime and moving towards clinical applications.
Keywords: MRI, NMR, Magnetic Resonance, Hyperpolarization, Low Field, Clinical Imaging

Introduction

Noninvasive clinical imaging modalities are useful diagnostic tools which can show pathological structures in the body. Some of the more widely used imaging techniques like x-ray radiographs, Computerized Tomography (CT), and mammograms use ionizing radiation to penetrate the skin and accent various internal structures. While the radiation inherent to modern implementations of these techniques is quite low, Magnetic Resonance Imaging (MRI) can achieve similar contrasts without the use of ionizing radiation.[13] However, there are several drawbacks to this technique including expensive up-front and maintenance, rapidly depleting resources, and dangerously high magnetic fields which can interfere with implanted medical devices.

MRI is a powerful clinical diagnostic technique which uses the fundamental property of nuclei called spin to generate detailed images of internal anatomy. If you consider the classical picture of a nucleus as a ball of positive charge, and spin this ball, you can approximate this as many concentric rings of positively charged current, each generating a magnetic moment pointing in the same direction. The net magnetic moment of the nucleus then either aligns with the applied field (spin up), or against the magnetic field (spin down) in the two energy equilibria, The difference between the number of spins occupying each of these states is the determining factor for the strength of the generated signal. The populations of spins in these states can be determined according to Eq. 1 where N_{down} and N_{up} are the number of spins in the spin down and spin up state respectively, B is the magnetic field, T is the temperature, $\hbar$ is Planck's constant, k is Boltzmann's constant, and γ is the gyromagnetic ratio of the nucleus, which defines the direct relationship between the magnetic field and the rotational frequency of the nucleus.[8]

$$\frac{N_{down}}{N_{up}} = e^{-\frac{\gamma\hbar B}{kT}} \quad [1]$$

The total population of each of these states is unimportant, as an MRI will only be able to detect the difference between these signals. Every spin up and spin down pair add no net magnetic moment to the bulk sample, so the pairs are essentially invisible to the MRI. Because of this, we generally consider the polarization (P) to be a more useful corollary to the detectable signal:

$$P = \tanh\left(\frac{\hbar\gamma B}{2kT}\right) \approx \frac{\hbar\gamma B}{2kT} \quad [2]$$

This polarization value will give the proportion of spins that are different between the populations and will therefore contribute to the signal.[15] For the protons in water at the magnetic field of the earth ($\sim 50\ \mu T$), this polarization is only 1.67×10^{-10}, so there has been a lot of work to date on generating large magnetic fields to directly increase the polarization of a spin sample. Modern imagers generally have a leading field B_0 of 1-3 T using a superconducting magnet. If we calculate the polarization of the same sample in a 3T imager, we now have a polarization of 1×10^{-5}. This value is much larger than the polarization at earth's field, but are still quite low. In fact, the largest preclinical imager to date at 11.7 T only

generates a polarization of 4×10^{-5}.[18] We are limited in how high we can raise the leading field and there are several problems with continuing to push the technology in this direction. These superconducting magnets increase the polarization linearly with the magnetic field, but the cost actually increases exponentially. In addition, because the superconducting materials used in these magnets need to be kept at $\sim 4\ K$, liquid helium (a rapidly depleting resource) is needed in large quantities.[18] For these reasons, MRI technology has been investigating lower, steady state magnet fields for reduction in cost and upkeep.

Advances in post-acquisition processing and hyperpolarization techniques have allowed for lower magnetic fields to achieve similar resolution as higher field magnets, allowing for less costly and more potential portability of imagers.[20] The 64 mT Hyperfine MRI which has recently been approved by the FDA for bedside imaging is one example of how far this development has come.[6,17] A natural partner with the growing low-field imaging field is hyperpolarization, a technique which artificially induces large differences in spin populations to increase the SNR regardless of the field.[14] Spin polarizations of close to 70% have been achieved in stark contrast with the 0.001% polarizations in modern imagers.[4] Some hyperpolarization techniques have already reached clinical applications. Dissolution Dynamic Nuclear Polarization (dDNP), is currently in clinical trials as a diagnostic tool for prostate cancer detection[12] and Spin Exchange Optical Pumping is revolutionizing clinical characterization of lung pathologies.[11] However, these techniques are limited by prohibitive cost, or the need for specialized personnel to operate equipment.

One alternative would be Signal Amplification By Reversible Exchange (SABRE) which is cheap and easy to implement. SABRE uses an iridium catalyst to bring together parahydrogen (a polarization source) and a target nucleus on a molecule of interest and transfers polarization out of the parahydrogen state and into the spin up state of the target nucleus. The original implementation of SABRE transferred this hyperpolarization to a target proton nucleus (^{1}H).[1] Since that time, the technique has proliferated and extended heteronuclear SABRE (X-SABRE)[5,10,16] has expanded on the potential nuclear targets to ^{31}P, ^{19}F, ^{13}C, and ^{15}N which have longer polarized lifetimes and very little background signal in the human body compared to ^{1}H.[2,3,7,16]

The X-SABRE technique which generates the most polarization is SABRE SHEATH, where a very low magnetic field is used to induce polarization transfer to a target nucleus.[16] There are many variables that

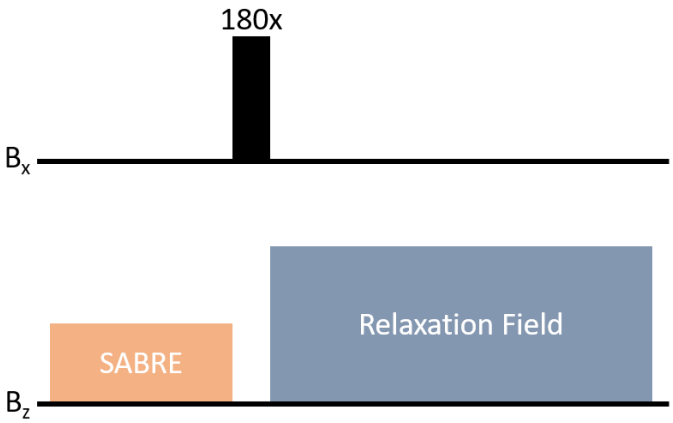

Fig. 1. Inversion Recover Experimental Pulse Sequence. An inversion recovery experiment requires pulses along the z and x axes. The z axis applies a polarization field, then a 180x pulse is applied along the x axis, which is then followed by a field for T1 relaxation.

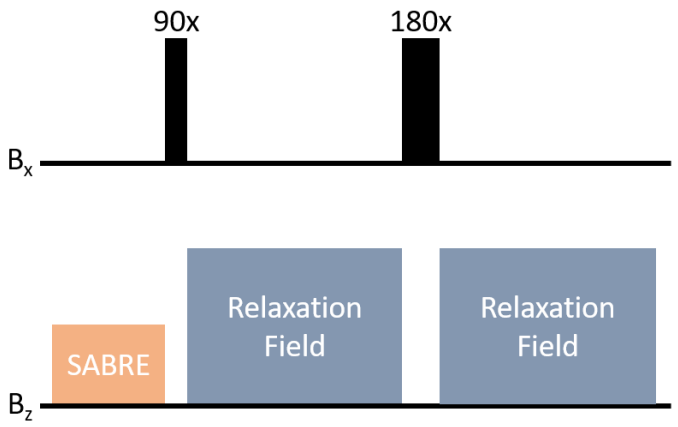

Fig. 2. Spin Echo Experimental Pulse Sequence. A spin echo experiment requires pulses along the z and x axes. The z axis applies a polarization field, then a 90x pulse is applied along the x axis, then a relaxation field is applied along the z axis, then a 180x pulse is applied along the x axis, which is then followed by another relaxation field along the z axis.

alter the generation of polarization in SABRE experiments including sample composition, spin coupling of the target molecule, chemical kinetics, and magnetic field among others. Variations between electromagnetic set-ups and various system parameters leads to a variety of polarization strategies in different labs. However, there is a new numerical simulation technique from the Warren lab which can predict optimal conditions and provide a physically accurate representation of the build up of spin polarization in a given sample.[9] This package can be used to not only optimize current SABRE methods, but also to introduce and determine appropriate quantities for basic NMR pulses and experiments.

Here, I will focus on implementing two traditional NMR experiments important in medical imaging: Inversion Recovery (IR) and Spin Echo (SE). Inversion Recovery experiments use the NMR pulse sequence shown in Figure 1 to measure a magnetic parameter called T_1 relaxation, also known as spin-lattice or longitudinal relaxation. The spin sample is polarized along the +z direction to generate only $\widehat{M}_z$ magnetization, then, some pulse in the x direction rotates the magnetization into the -z direction (180_x pulse) and the T_1 relaxation will then cause the magnetization to return to its equilibrium along the +z direction. Spin Echo experiments use the NMR pulse sequence shown in Figure 2 and are used to measure the magnetic parameter called T_2 relaxation, also known as spin-spin or transverse relaxation. The spin sample is once again polarized along the +z direction, then a 90_x pulse brings $\widehat{M}$ down into the transverse plane where T_2 relaxation causes the spins to rotate at different frequencies and decohere. Then application of a 180_x pulse inverts the spins in the transverse plane and the different frequencies of rotation then cause the spins to recohere and create what is called an echo. The magnitude of this echo can be used to determine how quickly the spins are decohere to get a measure of T_2.[8]

Overcoming the complexity of a hyperpolarization technique such as SABRE has the potential of lowering the barrier to entry for labs to engage in the development of this up and coming technique. The goal of this paper is the development of a relatively simple and self-contained set of tools to give labs the ability to use SABRE as an experimental technique with a cheap and reproducible experimental apparatus with calibrated inversion and excitation pulses for use in any number of low field NMR experiments. The example pulse sequences used in this paper

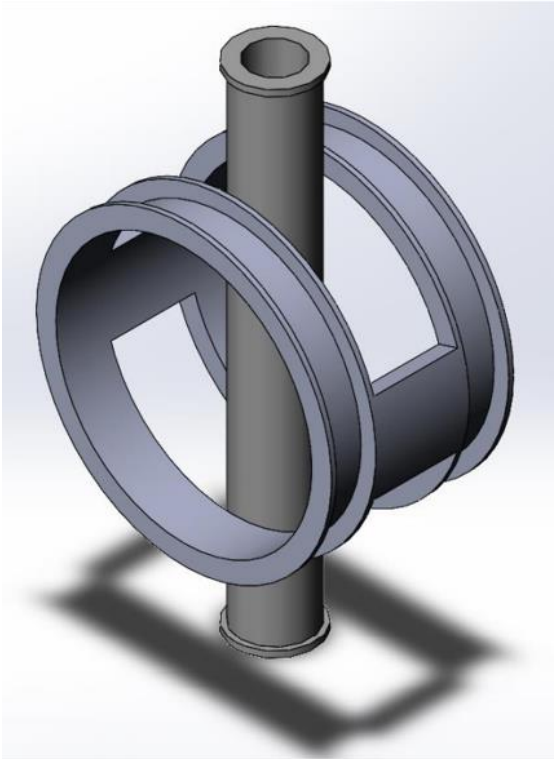

Fig. 3. CAD Design of Solenoid and Helmholtz Coil. The Helmholtz coil and solenoid designs as seen in CAD software. The solenoid is the vertical tube and the Helmholtz coil is the large pair of loops perpendicular to the solenoid.

will be the inversion recovery and spin-echo experiments, but the optimized pulses can be used in any number of basic NMR pulse sequences and even in optimization of the polarization transfer process of SABRE.

Results

Determining Electromagnet Parameters and Designing Array

The set of electromagnets was first designed in CAD software. To apply a SABRE polarization field and rotation pulses, two electromagnets operating in perpendicular directions were the components of this set. To allow these electromagnets to apply homogenous fields in the same region of space, the electromagnet for application of rotation pulses was decided to be a Helmholtz coil. This way, a solenoid could be designed to fit in between the two loops of the Helmholtz coil as shown in Figure 3.

The restricting dimension for the Helmholtz coil was decided to be the top-down diameter of the metal shield used in Dr. Warren's lab, which is 152mm. The dimensions of the solenoid were determined after the designing of the Helmholtz coil, since the space in between the two loops of the Helmholtz coil was the restricting dimension for the solenoid.

Helmholtz coils are typically designed with the dimensional constraint $r = d$ in mind, where r is the radius of the two loops and d is the distance between the two loops. Using the top-down diameter of the metal shield, the Helmholtz coil dimensional restraint, and some basic trigonometry, an expression for the maximum possible loop radius can be derived. This expression works out to be $D_{td}/\sqrt{5}$, where D_{td} is the top-down diameter. Since this expression assumed an ideal Helmholtz coil, and the real coil design included support features such as walls around the loops and structural support, the target diameter was reduced by 20% to accommodate. Performing the calculation for the loop radius with this in mind gives a radius of 54mm. The final Helmholtz coil design had a maximum top-down width that was approximately 10% smaller than the top-down diameter of the metal shield when including external design features.

The solenoid dimensions were worked out from the internal Helmholtz coil dimensions. The distance between the Helmholtz coil loops was 34mm after design was finished. This value represents the maximum possible diameter of the solenoid with the width of the wiring included. A solenoid coil was designed in CAD with caps at both ends that had a diameter equal to the distance between the Helmholtz coil loops. The radius of the solenoid everywhere besides these end caps was slightly reduced to account for wire width. The solenoid was designed in CAD in case users would prefer to 3D print it, however a PVC pipe with a diameter lower than 34mm would be suitable for use as well. Users would be encouraged to use a pipe over the 3D printed solenoid, since the PVC pipe can create a solenoid that is long enough to approximate an infinite solenoid. Since the radius is not a variable in this approximation, pipes with varying radii can be used.

When determining the number of wire turns to have in each Helmholtz coil loop and the solenoid, the maximum desired magnetic field was the primary concern. When designing the interface, the maximum required inversion pulse field was always 600μT or less. The number of turns in each Helmholtz coil loop was calculated with fields of 600μT or more in mind. The calculation assumed a current of 1A and used the Helmholtz coil loop radius of 54mm. Having 50 turns of wire in each loop of the Helmholtz coil resulted in a theoretical magnetic field of ~800 μT, which is well above the minimum value using a very reasonable current. The number of turns per cm required for the solenoid was based on a solenoid in Dr. Warren's lab that is used for experimentation. The solenoid has 15 turns per cm which results in a theoretical magnetic field of >1000 μT at 1A current.

Evaluating Reproducibility of the Coils

One important metric to look at for the printed coil set is reproducibility. There are two important measures of field reproducibility. First, it must be demonstrated that the field produced by each electromagnet (both the Helmholtz coil and the solenoid) varies linearly with the applied voltage according to Faraday's Law of Induction. To accomplish this, the Helmholtz coil and solenoid were wound the Helmholtz coil and solenoid as detailed above and a gaussmeter was used to measure the magnetic

Coil	Trial	slope (μT/V)	95% CI (μT/V)	p-value
Helmholtz Coil	A	256	{253, 259}	1.39E-35
	B	255	{252, 257}	5.70E-38
	C	256	{253, 258}	7.31E-37
Solenoid	A	298	{295, 301}	4.89E-44
	B	297	{294, 300}	8.58E-44
	C	297	{295, 300}	2.98E-44

Table. 1. Linear Regression of Field Measurements. Statistical measure for linear regression models of triplicate measurements of magnetic field vs voltage for electromagnetic coils.

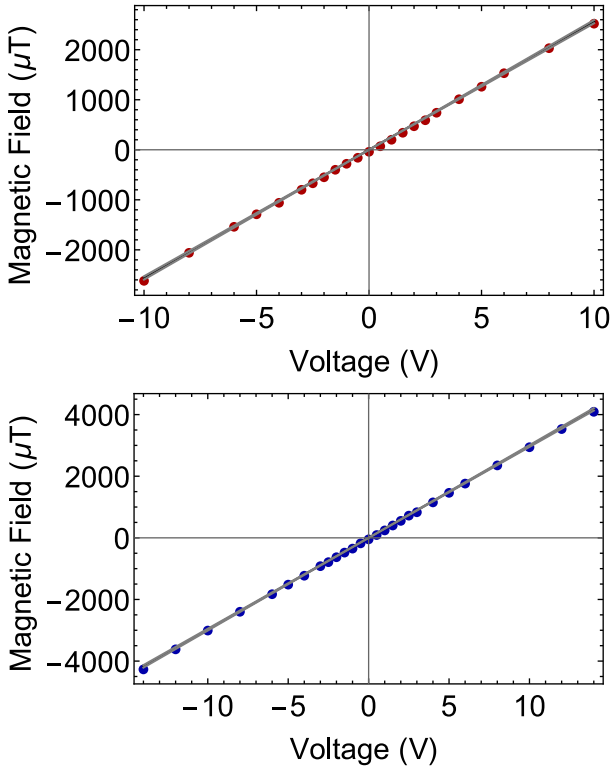

Fig. 4. Magnetic Field vs. Voltage Data and Regression. Field measurements at different voltages for the Helmholtz coil (red) and solenoid (blue) as well as linear fits for these data are shown.

field generated by the coil as a function of the applied voltage. A linear regression of this relationship was performed to determine the slope and assess the linear fit. These data and the linear regression can be seen in Figure 4. The p-value for the first wrapped coils were 1.39×10^{-35} for the Helmholtz coil and 4.89×10^{-44} for the solenoid (Table 1) indicating that the regression was statistically significant, and that the linear relationship was strict, as anticipated.

The second measure of reproducibility addresses potential variability introduced from winding of the electromagnet by the experimenter. The 3D printed electromagnet scaffold must be wound by the experimentalist which will naturally introduce potential variability. For this reason, the coils were wound three times each and the same measures were performed of the magnetic field as a function of applied voltage. There is substantial overlap in the 95% confidence intervals for each of the rewound Helmholtz coils in and solenoids in Table 1 indicating that there is not a statistically significant difference between the rewound coils, so long as the same type of wire is used in the winding.

It is important that these values are reproducible between coils because small changes in the field lead to large changes in the experimental outcome. Slight deviations in the z field generated by the solenoid will reduce the efficacy of SABRE polarization transfer which has a narrow window of optimization at $\sim \pm 0.5\,\mu T$ for a ^{15}N target molecule for example. At just 2 μT, polarization transfer is almost negligible. For the x field, differences in the field strength would lead to suboptimal inversion and excitation pulses which would decrease the effectiveness of the theoretically optimized pulse output.

Designing a User Interface

The first consideration when creating the user interface for the SABRE simulation package was what system variables should be taken in as inputs. The code that creates experimental systems is quite expansive for someone unfamiliar with it, and much of it is not necessary to understand unless you are creating a completely custom system from the ground up. To facilitate use of the code without a major time investment, the parts of the setup code that were of most importance were extracted and put into an interface with an approachable form. The variables that are most subject to change between systems are the polarization target, rate constants, and J-couplings.

The capability to change the polarization target was included as a dropdown menu with 4 nuclei that have been previously hyperpolarized by SABRE. These 4 nuclei are 15N, 13C, 19F, and 31P. When one of these nuclei is input by the user, it tags cells that are associated with the system setup of that nucleus. The system setup of that nucleus is then run before any optimization in the notebook runs.

The capability to change the rate constants was included as a number input field. The rate constants that are asked for in the interface are the k_{dX} and k_{aH}, which are the disassociation constant of nucleus X from the catalyst and the association constant of hydrogen to the catalyst respectively. These variables are saved and then used in system evaluation cell for the previously chosen target nucleus.

The capability to change the J-couplings was included as a number input field. The J-couplings that are asked for in the interface are the J_{XH} and the J_{HH}, which are the J-coupling between the target nucleus and its opposite hydrogen nucleus and the J-coupling between the two hydrogen nuclei in the bound hydrogen molecule.

The next set of variables that were added to the user interface were the experimental variables. These are the variables that will dictate timings and field strengths that are not optimized by the interface because they are independent variables. These variables are the polarization time, relaxation time, echo time, and relaxation field. These inputs are used when optimizing experiments and automatically outputting CSV files for use in waveform generators, both of which will be discussed later.

The capability to change the polarization time was included as a number input field. This represents the time the sample can polarize before relaxation occurs. The capability to change the relaxation and echo times was included as number input fields. These are times that must be changed over the course of multiple measurements for T_1 and T_2 experiments, respectively. The capability to change the relaxation field was included as a number input field. This variable represents the field at which relaxation will be allowed to occur during the experiment.

The last set of variables that were added to the user interface were the coil and file variables. The coil variables represent the relationship between magnetic field strength of the electromagnets and input voltage over the user's circuit. The file variable represents the prefix of any files output for use in experimentation. These variables are used only in the CSV file generation. The capability to change the coil variables was included as number input fields. The capability to change the file prefix was included as a text input field.

The major functions in the SABRE simulation package perform simulated experiments based on initial condition, system, and pulse sequence inputs. Pressure to make functions that have more specific purposes in this package has been low since the freedom to customize the basic functions for specific research questions is much more practical when looking into niche effects. To facilitate experimentation based on SABRE as a polarization technique, variables put into the user interface are used to automatically optimize the polarization field and rotation pulses that are commonly used.

One of the key things optimized by the interface after the user inputs variables is the SABRE polarization field strength. The nucleus type, rate

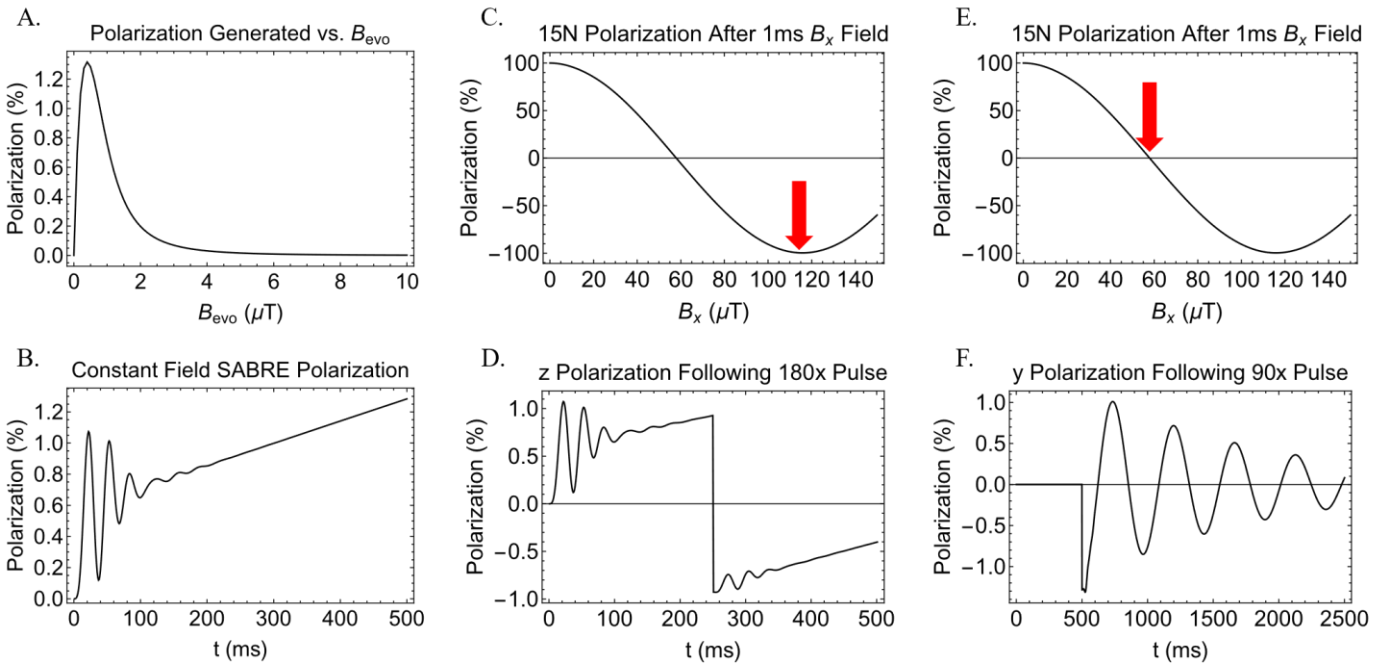

Fig. 5. SABRE Interface Output Plots. (A) A plot of polarization generated during a 500ms SABRE experiment performed at various fields. (B) A plot of a 500ms SABRE experiment performed at the optimal field. (C) Polarization of a 100% polarized sample of ^{15}N after a 1ms pulse at various x-axis magnetic fields with the inversion point highlighted. (D) A plot of a 500ms SABRE experiment performed at the optimal field with an inversion pulse at 250ms. (E) Polarization of a 100% polarized sample of ^{15}N after a 1ms pulse at various x-axis magnetic fields with the 90-degree rotation point highlighted. (F) Polarization in the y-axis during a 500ms SABRE experiment performed at the optimal field after a 90-degree rotation pulse.

constants, J-couplings, and polarization period time are all used in an experiment simulation function to produce a table of experimental results corresponding to a range of SABRE polarization fields. The final entry in each simulated experiment is taken as the final polarization after using a particular SABRE polarization field for the time the user entered as the polarization period. Using a function to find the position of the maximum value in this table allows us to identify the polarization field that generated the most polarization.

The 180x and 90x rotation pulses are commonly used pulses in NMR and MRI application. These pulses are also optimized by the interface for experimental use. In each nuclei's system setup cell, the equations $2\pi(B)(0.001s)(\gamma_x) = \pi$ and $2\pi(B)(0.001s)(\gamma_x) = \pi/2$ are solved for B, where B is the magnetic field and γ_x is the gyromagnetic ratio of the target nuclei. The B values output by these two equations correspond to 1ms 180x and 90x square wave pulses, respectively.

To use the optimized magnetic fields with the electromagnet set the field values must be converted into voltages and made into a waveform. The CSV file type can be uploaded into waveform generators to create custom waveforms. Using user input times and pulse magnetic field values, the magnetic fields at each time point through a T_1 and T_2 measurement experiment can be generated in a CSV format. By using the user input magnetic field to voltage ratio for each electromagnet the CSV file can be converted into voltages. Two CSV files are output into the user's documents file with the prefix that they input.

After optimization and CSV creation is completed, the immediate outputs are plots that give the user more insight into the optimization of pulses and the waveforms of the CSV files. Some additional functions are run to produce a couple of plots that allow the user to visually confirm that each individually optimized portion of the experimental sequence is working properly. A plot of the optimized polarization period over time is created using optimized values and an experimental simulation function. Plots of the 180x and 90x pulses inverting polarization and knocking polarization into the transverse plane are also created using two experimental simulation functions. The remaining plots showcase CSV files and SABRE polarization period optimization, as shown in Figure 5.

Using the Computational Interface with ^{13}C-pyruvate

As a test of the optimization the interface was used to produce values for a T_1 measurement experiment. The ^{13}C nucleus was chosen from the drop-down menu. The polarization period time was set to 500ms. The rate constants k_{dC} and k_{aH} were set as $16s^{-1}$ and $2s^{-1}$. The J-couplings J_{CH} and J_{HH} were set as $-24Hz$ and $-8Hz$. The relaxation field was set to $50\mu T$. The relaxation time varied over different measurements and the rest of the inputs were non-applicable since this T_1 measurement experiment was being carried out computationally. For each data point, polarization was generated, inverted, and then allowed to relax. Measurements were taken after letting the sample relax after a set amount of time ranging from 0s-60s. By fitting an inverse exponential to the data points, the T_1 could be found as the denominator of the exponent. The T_1 expected was 40s, since it was set in the code as such. The T_1 found from the simulated experiment using the interface values was 41.56s, which demonstrates that the interface produced a suitable experiment for simple and accurate T_1 measurement.

Discussion

SABRE hyperpolarization in combination with low field MRI are presenting an exciting opportunity for MR clinical imaging to reduce the cost and increase availability of this powerful diagnostic tool. However, because SABRE is a new scientific advancement, there is important groundwork which must be achieved in order to understand the experiment and look towards clinical applications. To reduce the variability between experiments and lower the barrier for new labs to begin SABRE experiments, I introduced rigorously reproducible and

theoretically optimized experimental apparatuses and protocols for some fundamental NMR experiments.

The numerical simulation package first introduced by the Warren lab provides a physically accurate representation of the evolution of arbitrary spin systems at the user's discretion.[9] Unfortunately, the format of the simulation code was not easily usable by anyone other than the graduate students who created it. By creating an easy to use interface, any experimenter can directly predict optimal conditions for SABRE experiments and generate exact experimental values which can be used in combination with a standard arbitrary waveform generator for application of excitation and inversion pulses. This theoretical optimization in combination with the 3D printable electromagnet scaffold and coil specifications which generates reproducible magnetic fields provides all of the necessary building blocks for running continuous field SABRE experiments as well as some basic NMR pulse sequences as demonstrated by the application to inversion recovery and spin echo sequences.

The overall start-up cost for running SABRE experiments in a new lab is relatively low as well. Because the CAD designs of the 3D printable electromagnet scaffolds are open access and 3D printers are available for use at many academic institutions, the construction of the magnetic coils for use in these experiments is simply the cost of the wire used to wrap the coils and any cost associated with using a 3D printer at a given institution. The estimated cost of the rest of the SABRE polarization unit is ~$5000 compared to the $2.5M price of the primary competing technology: DNP. Under the assumption that interested labs will already have access to an NMR, either through the academic institution, or as an instrument housed within the research group itself, the overall estimated cost of adding SABRE hyperpolarization capabilities to an existing NMR focused lab is only $3000. In addition, the use of the equipment and optimization technique put forward in this paper will mean more reproducibility and less variation between the field conditions in SABRE experiments across labs.

Unfortunately, because of the restricted availability of the lab space at Duke University during the COVID-19 pandemic, I was unable to perform some of the experimental verifications that I originally planned. Testing the application of these pulses in an experimental setting on a standard SABRE target like ^{15}N-acetonitrile would have allowed for more rigorous assessment of the protocol put forward. However, I was limited to assessing the optimization and application of the optimized pulses in a theoretical setting with a simulated molecule. Under these conditions, the theoretical experimental results recovered the assigned relaxation parameter as discussed previously.

There is significant room for growth for the optimization platform put forward in this thesis. The simplest addendum would be an expansion on the potential target molecules including various spin network connections. The current iteration allows for exchange of various nuclear targets, but substantial changes in the coding would allow for an expansion of the form of the target molecule. For example, the simulated pyruvate molecule used in the theoretical pulse sequences for this thesis includes a target ^{13}C with three J-coupled protons (^{1}H). This is one of several potential "J-coupling networks" that can be present in the target molecule. In the future, I could set up several variations on these coupling networks for users to input for more accurate representations of their target molecule.

In addition to direct extension of the existing user interface, I could incorporate some of the work I have been doing with shaped radiofrequency pulses at low field for highly selective excitation of specific nuclei. These selective pulses are often used in MRI pulse sequences and would be useful additions to the potential applications of this experimental protocol package. The direct application for this experimental set-up that would be most interesting to pursue would be optimization of the polarization transfer process in SABRE itself. Preliminary theoretical work shown in Figure 6 suggests that the addition of interleaved inversion pulses during a continuous field SABRE SHEATH experiment leads to dramatic improvements in the polarization, however the experimental apparatus to test this result has not been cheaply and easily available until now. With the addition of the 3D printed Helmholtz coil set-up for the application of magnetic fields in the x direction in combination with the solenoid field in the z direction, many new strategies for polarization transfer can be readily tested with experiment after promising theoretical results.

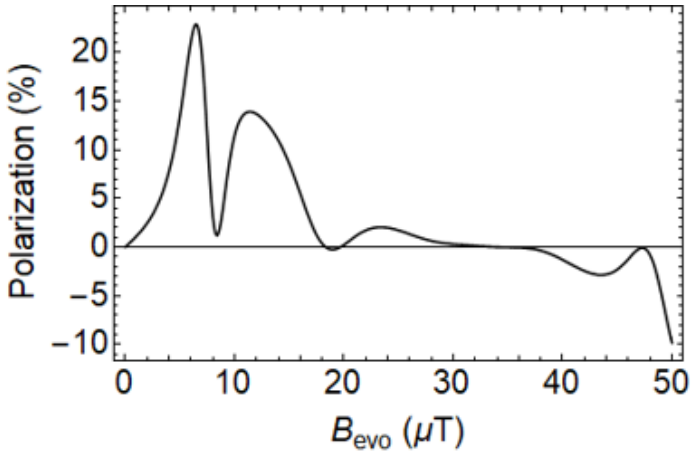

Fig. 6. Polarization of Constant Field SABRE Experiment With Interleaved Inversion Pulses. A plot of the polarization generated for a constant field SABRE experiment with 1ms inversion pulses spaced every 2ms vs the magnitude of the evolution field.

Because this thesis presents an experimental protocol which optimizes the building blocks for many NMR experiments, the possible applications are numerous and varied. This low-cost experimental apparatus and protocol make SABRE hyperpolarization more approachable and reproducible for any standard NMR spectroscopy lab. With increased input into the development of SABRE modalities, the work necessary to bring this technique to clinical application can be done much faster and the medical benefits of such an advancement can be realized quicker.

Materials and Methods

Designing, Creating, and Printing Electromagnet Set

The Helmholtz coil and solenoid CAD designs were created with SolidWorks CAD software using dimensional restraints dictated by lab equipment found in Dr. Warren's lab at Duke University. SolidWorks CAD software was used to output STL files for the Helmholtz coil. The STL file was then uploaded to an online 3D printing service available at Duke University, and the printed piece was acquired once printed. Supports were removed and the Helmholtz coil was wrapped with 50 turns of 24-gauge copper wire in each loop. An electromagnet created by a pipe wrapped with 24-gauge copper wire was used as the solenoid during measurement.

Coil Reproducibility Measurements

A high precision gaussmeter with an instrumental error of $\pm 0.1\ G$ or $\pm 10\ \mu T$ was secured in position with directionality perpendicular to the face of the Helmholtz coil, or fixed vertically in the center of the bore of the solenoid. Banana clips were affixed to each terminal of each coil and the resistance of each coil was measured with a multimeter. A standard DC current power supply capable of delivering up to 4 A of current was used to drive the coil directly. The voltage output of the power supply was varied from -14V to +14V with the terminals of the coil plugged directly into the power supply. The measurement from the gaussmeter was recorded at each voltage. This procedure was repeated for each coil, then the coils were re-wound 2

additional times and the experiment was repeated again. A linear regression was performed in Mathematica to determine the slope of the relationship between the field and voltage and the confidence interval for that slope was calculated for comparison to the other iterations of each coil.

Construction of The User Interface in Mathematica

The SABRE simulation package is based in Mathematica. By customizing system setups from this Mathematica package and giving each system setup a unique cell tag, buttons in the interface were coded in to run the system setup associated with the user's target. Numerical inputs were saved as dynamic variables in the notebook, which would update every time the user changed them. When these inputs were updated, the notebook ran relevant cells again to ensure all code is up to date. The Mathematica function Export was used to export a table constructed by code as a CSV into the user's default save location for Mathematica. All optimization was done using the SABRE simulation package's experiment functions.

Simulation of 13C-pyruvate T_1 Measurement

The user interface was used to provide an optimized constant field SABRE polarization field, along with field strengths required for 1ms 180x and 90x rotation pulses. The inputs to the system were as follows. The nucleus was 13C. The k_{dC} and k_{aH} were 16^{-1} and 2^{-1}. The J_{CH} and J_{HH} were $-24Hz$ and $-8Hz$. The relaxation field was $-50\mu T$. A new Mathematica notebook was created for the purpose of simulating a more physically accurate ^{13}C-pyruvate experiment. Using the custom setup for ^{13}C-pyruvate and interface outputs, an inversion recovery experiment was run with a relaxation period of 60s. Data points were collected from every 5s of the relaxation period. By fitting the data to an inverse exponential with the form ae^{-bt} where $T_1 = 1/b$, the T_1 was measured from the data.

End Matter

Author Contributions and Notes

Clark W. Eriksson designed research, Clark W. Eriksson performed research, Clark W. Eriksson wrote software, Clark W. Eriksson analyzed data; Clark W. Eriksson wrote the paper.
The authors declare no conflict of interest.

Acknowledgments

I would like to thank Dr. Warren S. Warren and his graduate student Jacob R. Lindale for mentoring me and monitoring the progress of this project.

References

1. Adams, R. W., Aguilar, J. A., Atkinson, K. D., Cowley, M. J., Elliott, P. I., Duckett, S. B., ... & Williamson, D. C. (2009). Reversible interactions with para-hydrogen enhance NMR sensitivity by polarization transfer. *Science*, 323(5922), 1708-1711.
2. Ariyasingha, N. M. *et al.* Quasi-Resonance Fluorine-19 Signal Amplification by Reversible Exchange. *The journal of physical chemistry letters* **10**, 4229-4236 (2019).
3. Burns, M. J. *et al.* Improving the hyperpolarization of 31P nuclei by synthetic design. *The Journal of Physical Chemistry B* **119**, 5020-5027 (2015).
4. Capozzi, A., Patel, S., Wenckebach, W. T., Karlsson, M., Lerche, M. H., & Ardenkjær-Larsen, J. H. (2019). Gadolinium Effect at High-Magnetic-Field DNP: 70% 13C Polarization of [U-13C] Glucose Using Trityl. *The journal of physical chemistry letters*, *10*(12), 3420-3425.
5. Colell, J. F., Logan, A. W., Zhou, Z., Shchepin, R. V., Barskiy, D. A., Ortiz Jr, G. X., ... & Theis, T. (2017). Generalizing, extending, and maximizing nitrogen-15 hyperpolarization induced by parahydrogen in reversible exchange. *The Journal of Physical Chemistry C*, 121(12), 6626-6634.
6. Cooley, C. Z., Stockmann, J. P., Armstrong, B. D., Sarracanie, M., Lev, M. H., Rosen, M. S., & Wald, L. L. (2015). Two-dimensional imaging in a lightweight portable MRI scanner without gradient coils. *Magnetic resonance in medicine*, 73(2), 872-883.
7. Gemeinhardt, M. E. *et al.* "Direct" 13C Hyperpolarization of 13C‐Acetate by MicroTesla NMR Signal Amplification by Reversible Exchange (SABRE). *Angewandte Chemie* **132**, 426-431 (2020).
8. Levitt, M. H. (2013). Spin dynamics: basics of nuclear magnetic resonance. John Wiley & Sons.
9. Lindale, J. R., Eriksson, S. L., Tanner, C. P. N., & Warren, W. S. (2020). Infinite-order perturbative treatment for quantum evolution with exchange. *Science advances*, 6(32), eabb6874. doi:10.1126/sciadv.abb6874
10. Lindale, J. R., Eriksson, S. L., Tanner, C. P., Zhou, Z., Colell, J. F., Zhang, G., ... & Warren, W. S. (2019). Unveiling coherently driven hyperpolarization dynamics in signal amplification by reversible exchange. *Nature communications*, 10(1), 1-7.
11. Möller, H. E., Chen, X. J., Saam, B., Hagspiel, K. D., Johnson, G. A., Altes, T. A., ... & Kauczor, H. U. (2002). MRI of the lungs using hyperpolarized noble gases. *Magnetic Resonance in Medicine: An Official Journal of the International Society for Magnetic Resonance in Medicine*, *47*(6), 1029-1051.
12. Nelson, S. J., Kurhanewicz, J., Vigneron, D. B., Larson, P. E., Harzstark, A. L., Ferrone, M., ... & Reed, G. (2013). Metabolic imaging of patients with prostate cancer using hyperpolarized [1-13C] pyruvate. *Science translational medicine*, 5(198), 198ra108-198ra108.
13. Nelson, J. H. (2003). Nuclear Magnetic Resonance Spectroscopy. Prentice Hall.
14. Nikolaou, P., Goodson, B. M., & Chekmenev, E. Y. (2015). NMR hyperpolarization techniques for biomedicine. Chemistry (Weinheim an der Bergstrasse, Germany), 21(8), 3156–3166. https://doi.org/10.1002/chem.201405253
15. Tateishi, K., Negoro, M., Nishida, S., Kagawa, A., Morita, Y., & Kitagawa, M. (2014). Room temperature hyperpolarization of nuclear spins in bulk. *Proceedings of the National Academy of Sciences*, 111(21), 7527-7530.
16. Theis, T., Truong, M. L., Coffey, A. M., Shchepin, R. V., Waddell, K. W., Shi, F., ... & Chekmenev, E. Y. (2015). Microtesla SABRE enables 10% nitrogen-15 nuclear spin polarization. *Journal of the American Chemical Society*, 137(4), 1404-1407.
17. Tyszka, J. M. (2021). Compact brain MRI. *Nature Biomedical Engineering*, *5*(3), 201-202.
18. Vedrine, P., Aubert, G., Belorgey, J., Berriaud, C., Bourquard, A., Bredy, P., ... & Sinanna, A. (2013). Manufacturing of the Iseult/INUMAC whole body 11.7 T MRI magnet. *IEEE* Transactions on Applied Superconductivity, 24(3), 1-6.
19. Zhivonitko, V. V., Skovpin, I. V. & Koptyug, I. V. Strong 31 P nuclear spin hyperpolarization produced via reversible chemical interaction with parahydrogen. *Chemical Communications* **51**, 2506-2509 (2015).
20. Zhu, B., Liu, J. Z., Cauley, S. F., Rosen, B. R., & Rosen, M. S. (2018). Image reconstruction by domain-transform manifold learning. *Nature*, 555(7697), 487-49